Available online at www.sciencedirect.com

ScienceDirect

IFAC PapersOnline CONFERENCE PAPER ARCHIVE

IFAC PapersOnLine 55-4 (2022) 189–194

Dynamic Equivalent Circuit Models of Lead-Acid Batteries – A Performance Comparison

Mateo Bašić*, Dinko Vukadinović*, Vice Višnjić*, Ivan Rakić*

**University of Split, Faculty of Electrical Engineering, Mechanical Engineering and Naval Architecture, Split, Croatia (Tel: +385 21 305 615; e-mail: mabasic@fesb.hr, dvukad@fesb.hr, vvisnj00@fesb.hr, irakic00@fesb.hr)*

Abstract: This paper presents a performance comparison of the four most commonly used dynamic models of lead-acid batteries that are based on the corresponding equivalent circuit. These are namely the Thevenin model, the dual polarization (DP) model (also known as the improved Thevenin model), the partnership for a new generation of vehicle (PNGV) model, and the general non-linear (GNL) model. The equivalent circuit models (ECMs) are widely used for modeling, simulation, and state-of-charge (SOC) estimation of battery systems due to the fact that the physical variables in ECMs are easily understood and intuitive. The parameters of the ECMs may be modeled as constant or as dependent on the battery condition indicators, such as the SOC, temperature, state of health (SOH), operating regime, etc. In this study, the values of the ECM parameters have been determined from the pulse-charge and pulse-discharge tests conducted at five different SOC levels within the range 50%-90% and then approximated by second order polynomial functions. The corresponding simulation models have been developed in the MATLAB Simulink environment, whereas their accuracy has been evaluated based on the comparison with the experimental results acquired and processed by means of the DS1104 controller board (dSpace).

Keywords: Equivalent circuit model, Dynamic analysis, DS1104 controller board, Lead-acid battery, MATLAB-Simulink.

1. INTRODUCTION

Batteries are the most prominent energy-storage devices today due to their high efficiency and low pollution. They are commonly used in portable devices, electrified transportation, industrial applications, etc. (Hu et al., 2016; Huang et al., 2014). The most common types of rechargeable batteries include lead-acid, Ni-Cd, Ni-MH, and Li-ion batteries. The selection of a battery type is conditioned by the energy storage requirements of a specific application. Lead-acid (LA) batteries are commonly used in renewable energy systems (Chiu et al., 2011), due to the fact that they are relatively cheap, easily transported, and available in wide range of sizes and specifications.

Battery condition indicators such as the state of charge (SOC) and state of health (SOH) are of utmost importance for battery monitoring and control. However, they cannot be directly measured, so they have to be inferred from the battery model. Their estimation is complicated by the fact that they are affected by the operating conditions (temperature, charge/discharge rate, etc.), so to obtain accurate estimates in real-time, it is important to strike a balance between model complexity and accuracy.

Electrochemical battery models (Doyle, Fuller, and Newman, 1993; Haran, Popov, and White, 1998) are based on partial differential equations accounting for the dynamics of particles inside the battery. Albeit highly accurate, these models are quite complex and require knowledge of a large number of parameters which are difficult to obtain. Data-driven models allow establishing the relationship between the battery variables through analysis of the collected data from previous applications (Du, Liu, and Wang, 2014). However, their accuracy is dependent on the training dataset. Empirical models (Moore and Eshani, 1996; Unnewehr and Nasar, 1982; Fang et al., 2014) are simplified electrochemical models in which the terminal voltage is defined as a mathematical function of the current and the SOC. However, they are valid only for specific applications, with the relative error ranging from 5% to 20% (Chen and Rincon-Mora, 2006). Equivalent circuit models (ECMs) are most widely used for battery modeling, simulation, and SOC estimation. They provide the optimum balance between accuracy and complexity, whereas the physical variables in ECMs are easily explained and understood (He, Xiong, and Fan, 2011; Meng et al., 2018; Zhou et al., 2021). These models are typically composed of resistors, capacitors, and ideal voltage sources. The simplest ECM is known as the Rint model, consisting only of an ideal voltage source and a series resistance. However, it cannot describe well the battery dynamics since it does not include the polarization effect. As for the dynamic ECMs, the four most common are the Thevenin model, the dual polarization (DP) model (i.e., the improved Thevenin model), the partnership for a new generation of vehicle (PNGV) model, and the general non-linear (GNL) model, which are described in the next section.

In this paper, the simulation models of the four most common dynamic battery ECMs are built in the MATLAB-Simulink environment and evaluated based on the comparison between the simulation and experimental voltage responses. Two

10.1016/j.ifacol.2022.06.031

approaches are considered with regard to the parameter representation: one with constant ECM parameters and the other with the ECM parameters considered as variable with respect to the SOC and charging/discharging operation. Similar approach was adopted in (Rahmoun and Biechl, 2012), but only for the Thevenin and DP models, and without going beyond determining the model parameters, whereas the PNGV model proposed in (Castano et al., 2015) utilized the averaged values of the charging and discharging parameters. In this study, each of the resistive-capacitive (RC) parameters of the considered ECMs is determined separately for the charging and discharging operation and approximated by a second order polynomial function.

2. BATTERY EQUIVALENT CIRCUIT MODELS

2.1 Thevenin model

The Thevenin model, shown in Fig. 1, is obtained by adding a parallel RC network to the Rint model in order to include the polarization effect and to better describe the charging/discharging and recovery periods. The corresponding terminal voltage is defined as

$$U_b = U_{oc} - I_b R_0 - U_1 \tag{1}$$

where U_{oc} denotes the open-circuit voltage, R_0 denotes the internal series resistance, U_1 denotes the voltage across the polarization resistance (R_1) and capacitance (C_1), and I_b is the battery current having a positive value at discharging.

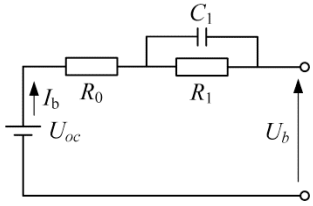

Figure 1. Equivalent circuit of the Thevenin model

2.2 Dual polarization model

By adding another parallel RC network to the Thevenin model, to differentiate between the electrochemical and concentrated polarization, the dual polarization (DP) model is obtained (Fig. 2).

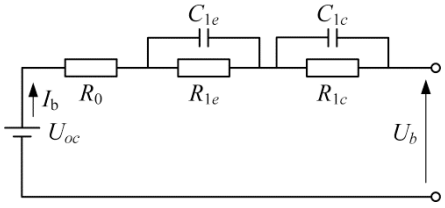

Figure 2. Equivalent circuit of the DP model

The corresponding terminal voltage is defined as

$$U_b = U_{oc} - I_b R_0 - U_{1e} - U_{1c} \tag{2}$$

where U_{1e} denotes the voltage across the electrochemical polarization resistance (R_{1e}) and capacitance (C_{1e}), whereas U_{1c} denotes the voltage across the concentrated polarization resistance (R_{1c}) and capacitance (C_{1c}).

2.3 PNGV model

Alternatively, a series capacitance C_0 can be added to the Thevenin model to describe the accumulative effect of the battery current on the open-circuit voltage, thus obtaining the PNGV model (Fig. 3).

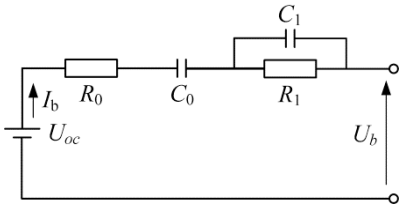

Figure 3. Equivalent circuit of the PNGV model

The corresponding terminal voltage is defined as

$$U_b = U_{oc} - I_b R_0 - U_1 - U_{C0} \tag{3}$$

where U_{C0} denotes the voltage across C_0.

2.4 GNL model

The fourth considered ECM, shown in Fig. 4, is obtained either by adding another parallel RC network to the PNGV model or by adding a series capacitance to the DP model. This model, known as the GNL model, has the largest number of parameters of all the considered ECMs, so it implies highest complexity. The corresponding equations are defined as follows:

$$U_b = U_{oc} - I_b R_0 - U_{1e} - U_{1c} - U_{1r} - U_{C0} \tag{4}$$

$$\frac{dU_{1e}}{dt} = -\frac{U_{1e}}{R_{1e}C_{1e}} + \frac{I_b}{C_{1e}} \tag{5}$$

$$\frac{dU_{1c}}{dt} = -\frac{U_{1c}}{R_{1c}C_{1c}} + \frac{I_b}{C_{1c}} \tag{6}$$

$$\frac{dU_{C0}}{dt} = \frac{I_b}{C_0} \tag{7}$$

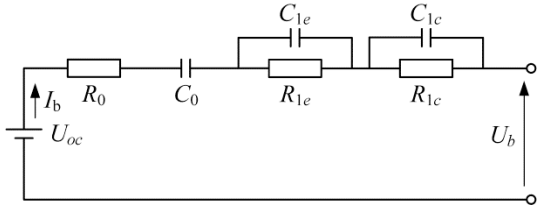

Figure 4. Equivalent circuit of the GNL model

The ideal voltage source in Figs. 3 and 4 may even be omitted, whereas the initial open-circuit voltage is then defined as the initial condition of C_0. Note also that all or some of the parameters of the above discussed ECMs may be modeled as dependent on the battery SOC, operating regime, temperature or state of health (SOH) to further increase the ECM's accuracy. In this study, the resistance and capacitance values of the considered ECMs are considered as variable with respect to the battery operating mode (charging or discharging) and SOC. The identification of the battery ECM parameters is described in the next section.

3. PARAMETERS IDENTIFICATION PROCESS

The parameters of the considered ECMs were determined from pulse-charge and pulse-discharge tests conducted at five SOC levels – 50%, 60%, 70%, 80%, and 90% – computed by the ampere-hour (Ah) integration method (He, Xiong, and Fan, 2011, Meng et al., 2018, Zhou et al., 2021). The tests were performed on a valve-regulated LA battery rated at 12 V / 75 Ah. The Magna-Power SL50-30/UI programmable source and the ITECH IT8615 programmable load were used to impose constant current charging and discharging, respectively. The battery terminal voltage and current were measured by means of the Hall-effect sensors LV25-P (LEM) and LA55-P (LEM), respectively. The measured data were processed by means of the DS1104 controller board (dSpace).

Each of the tests consisted of the following sequence: initial 2 minute resting period followed by 5 minute discharging with I_b = 7.5 A, 10 minute recovery period, 5 minute charging with I_b = –7.5 A, and 10 minute recovery. The initial open-circuit voltage ($U_{oc\text{-}init}$) was determined during the initial resting period. Fig. 5 shows the battery terminal voltage and current recorded for the tests performed at SOC = 70%.

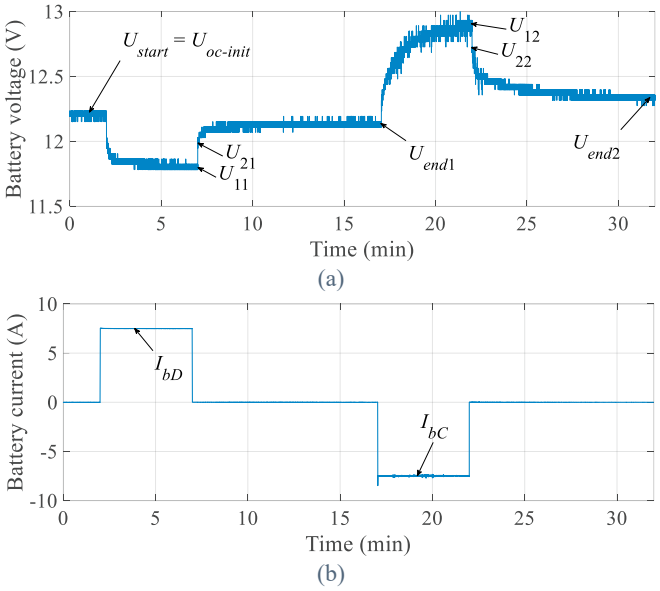

Figure 5. Measured battery terminal voltage (a) and current (b) during pulse-charge and pulse-discharge test at SOC = 70%

3.1 Series resistance identification

The series resistance, which is a common parameter to all the models considered in this study, is determined first as

$$R_{0D} = \frac{U_{21} - U_{11}}{I_{bD}}, \quad R_{0C} = \frac{U_{22} - U_{12}}{I_{bC}} \qquad (8)$$

where R_{0D} and R_{0C} denote the series resistances determined from the voltage step responses at the end of the discharging (from U_{11} to U_{21}) and charging (from U_{12} to U_{22}) intervals, respectively. The same $_D$ and $_C$ notation in the subscript is used for other ECM parameters as well.

Fig. 6 shows the R_{0D} and R_{0C} values as a function of the SOC. There is a notable increase of the series resistance with decreasing SOC. In addition, the values obtained by measurement can be reasonably well approximated by second order polynomial functions, which can then be utilized in the corresponding simulation model. The difference between the R_{0D} and R_{0C} values of a few milliohms may as well be neglected in some applications.

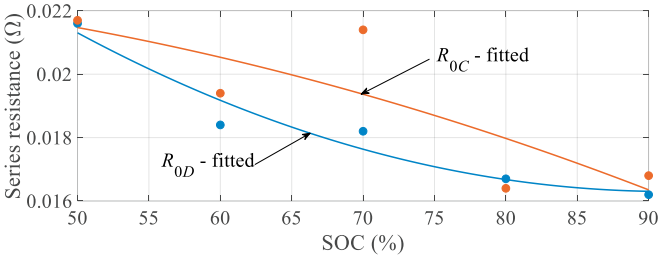

Figure 6. Series resistance values determined from the pulse-charge and pulse-discharge test at different SOC levels (all ECMs)

3.2 Identification of RC network parameters

The RC network parameters of the Thevenin model are determined from the voltage responses recorded during the recovery intervals following the discharging (U_{21} to U_{end1}) and charging (U_{22} to U_{end2}) of the battery. The coefficients of the exponential fitting functions applied to the recovery intervals of interest were determined by using the least squares method in MATLAB. The example in Fig. 7 shows the recovery interval following the battery discharging at SOC = 70%. The RC network parameters are calculated as

$$R_{1D} = A/(I_{bD}(1-e^{-t/T_1})), \quad C_{1D} = T_1/R_{1D} \qquad (9)$$

where A and T_1 are the coefficients of the exponential fitting function (Fig. 7), and I_{bD} is the discharging current.

The RC parameters for the recovery interval following the battery charging are determined in a similar manner, as well as the RC parameters at different SOC levels.

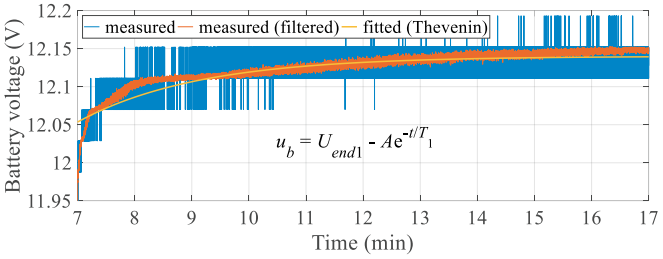

Figure 7. Single RC network approximation of the measured battery terminal voltage during the recovery interval following the battery discharging at SOC = 70% (Thevenin and PNGV)

Fig. 8a shows the R_{1D} and R_{1C} values, whereas Fig. 8b shows the C_{1D} and C_{1C} values as a function of the SOC. Second order polynomial approximation of the values obtained by measurement has been applied in this case as well. It can be observed that there is a notable difference between the values associated with charging and those associated with discharging. In addition, the R_{1D} and R_{1C} values seem to decrease with the SOC, whereas the C_{1D} and C_{1C} values reach their maximum in the region 60%-70%.

Note that the RC network parameters determined for the Thevenin model are also valid for the PNGV model.

Next, the RC network parameters of the DP model are determined from the same battery recovery responses as in the previous example. The example in Fig. 9 is given for the same recovery interval as in Fig. 7. The procedure is similar as that described for the Thevenin model, with the corresponding parameter equations given as follows:

$$R_{1eD} = A/(I_{bD}(1-e^{-t/T_1})), \quad C_{1eD} = T_1 / R_{1eD} \qquad (10)$$

$$R_{1cD} = B/(I_{bD}(1-e^{-t/T_2})), \quad C_{1cD} = T_2 / R_{1cD} \qquad (11)$$

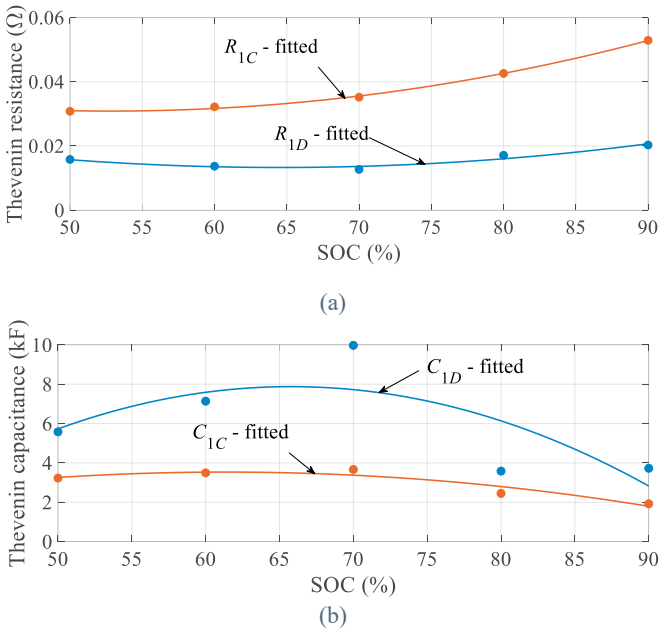

Figure 8. Single RC network resistance (a) and capacitance (b) values determined from the pulse-charge and pulse-discharge test at different SOC levels (Thevenin and PNGV)

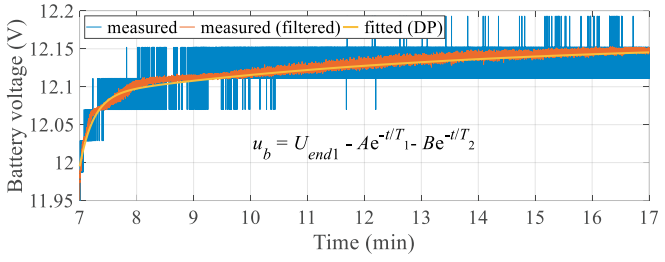

Figure 9. Dual RC network approximation of the measured battery terminal voltage during the recovery interval following the battery discharging at SOC = 70% (DP and GNL)

It is clear that the DP model provides a more accurate description of the voltage compared to the Thevenin model, but it also introduces an additional differential equation. Again, the RC parameters for the recovery interval following the battery charging are determined in a similar manner, as well as the RC parameters at different SOC levels (Fig. 10).

There is again a notable difference between the charging and discharging parameter values. In addition, the C_{1c} and R_{1c} values, describing the concentrated polarization, are notably larger than the C_{1e} and R_{1e} values, associated with the electrochemical polarization, thus yielding larger time constants. As in the Thevenin model, the polarization resistances seem to decrease with the SOC, whereas the capacitances reach their maximum in the region 60%-70%. Once more, the values obtained by measurement are well approximated by second order polynomial functions.

Note that the RC network parameters determined for the DP model are also valid for the GNL model.

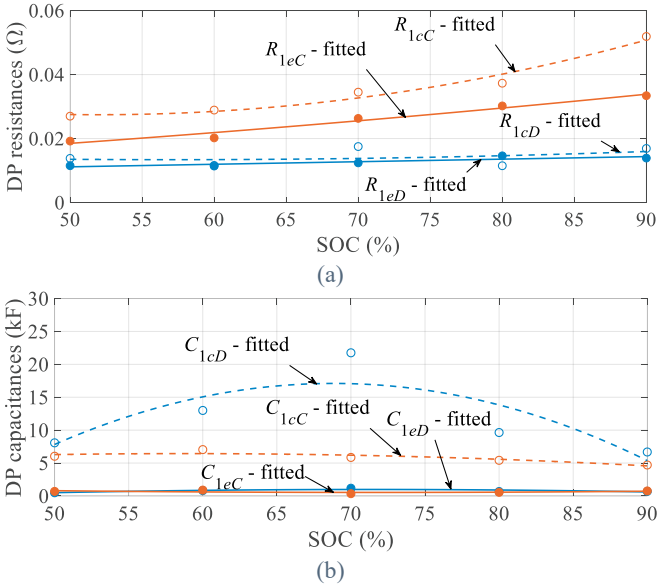

Figure 10. Dual RC network resistance (a) and capacitance (b) values determined from the pulse-charge and pulse-discharge test at different SOC levels (DP and GNL)

3.3 Series capacitance identification

The series capacitance is determined as the slope between the charge (ΔQ) and voltage variation (ΔU), where ΔQ can be expressed as a product of the battery current (I_b = 7.5 A in this study) and the time interval Δt during which the current is applied (Δt = 300 s in this study). The ΔU value is obtained as the difference of the open-circuit voltages between the beginning and the end of the charge and discharge intervals, including the battery recovery. All these values can be extracted from Fig. 5 as follows:

$$C_{0D} = \frac{I_{bD} \cdot \Delta t}{U_{start} - U_{end1}}, \quad C_{0C} = \frac{I_{bC} \cdot \Delta t}{U_{end1} - U_{end2}} \qquad (12)$$

Fig. 11 shows C_{0D} and C_{0C} as a function of the SOC.

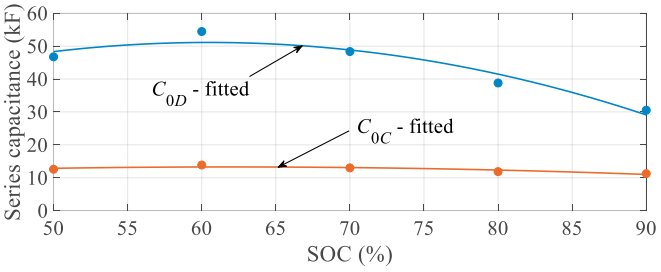

Figure 11. Series capacitance values determined from the pulse-charge and pulse-discharge test at different SOC levels (PNGV and GNL)

Second order polynomial fitting has been again applied. The fact that the C_{0D} values are 3-5 times larger than the C_{0C} values suggests that the ECM's accuracy may be significantly impaired by neglecting the dependency of C_0 on the battery operating regime. Note that the determined C_0 values are applicable to both the PNGV and GNL models.

4. RESULTS AND DISCUSSION

The simulation models of the considered battery ECMs were built in the MATLAB-Simulink environment. For each of the ECM configurations, two cases were considered regarding the parameter values: one in which the parameters were considered as constant and another in which they were considered as variable with respect to both the SOC and charging/discharging operation, with the parameters' values approximated by second order polynomial functions, as depicted in Figs. 6, 8, 10, and 11. Within the first approach, the parameter values were calculated as a mean average of the values determined from the pulse-charge and pulse-discharge tests performed at SOC = 70%, which represents the mean SOC value given the range considered. The resulting parameters' values are given in Table 1.

Table 1. ECM constant parameter values

R_0 (Ω)	C_0 (kF)	R_1 (Ω)	C_1 (kF)	R_{1e} (Ω)	C_{1e} (kF)	R_{1c} (Ω)	C_{1c} (kF)
0.020	30.7	0.024	6.82	0.019	0.76	0.026	13.9

Figs. 12 shows the simulation responses of the battery terminal voltage for the pulse-charge and pulse-discharge tests performed at two distinct SOC values: 60% and 80%. The simulation responses were obtained by the application of different ECMs and are presented along with the corresponding experimental responses. The charging and discharging currents were set to –7.5 A and 7.5 A, respectively, as in Fig 5b. To simplify the analysis, U_{oc} in the ECMs was set equal to the measured initial battery voltage (alternatively, $U_{oc} = f(\text{SOC})$ would have to be considered).

The impact of the parameter variation on the Thevenin and the DP model is only pronounced during transients, whereas the steady-state values of the terminal voltage are practically unaffected by it. The other two models are, on the other hand, largely affected by the parameter variation both during transients and at steady state, which is due to the existence of the series capacitance. The GNL model provides the most accurate estimation of the actual terminal voltage both during charging/discharging and recovery. The PNGV model fails to achieve the accuracy of the GNL model during charging or discharging, but it describes the recovery process equally well and results in the same open-circuit voltage as the GNL model (due to the common series capacitance). This feature is of great importance in applications that require knowledge of the exact open-circuit voltage value (e.g., SOC or SOH estimation). As for the other two models, the DP model describes the battery dynamics with higher accuracy compared to the Thevenin model, but they both provide insufficiently accurate estimation of the open-circuit voltage.

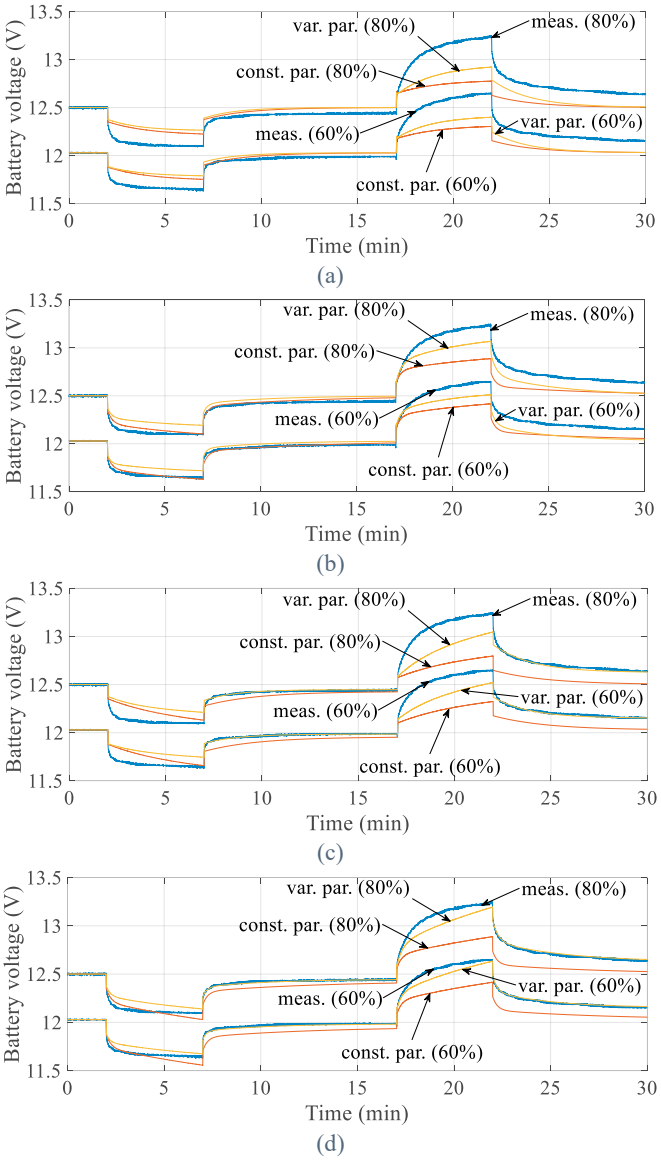

Figure 12. Voltage responses of the battery ECMs with constant and variable parameters for pulse-charge/discharge tests at SOC = 60% and SOC = 80%: (a) Thevenin, (b) DP, (c) PNGV, and (d) GNL

Two additional performance indicators were considered: the integral absolute error (IAE), which was calculated for all the considered ECMs based on the pulse-charge and pulse-discharge tests performed in the considered SOC range, and the simulation execution time (T_{sim}), which was obtained for the same tests. The results are presented in Fig. 13.

The most significant positive impact of parameter variation on the achieved accuracy is noted for the GNL model, with the IAE value reduced by about four times. The IAE of the PNGV model is reduced by more than twice, whereas this difference is somewhat less pronounced in the Thevenin and DP models. Furthermore, it is observed in Fig. 13 that the addition of the series capacitance to the Thevenin model contributes more to the overall accuracy than the addition of another RC network. Still, the combination of these two actions results in the most accurate, GNL model (the corresponding IAE value is about twice lower compared to the next most accurate, PNGV model).

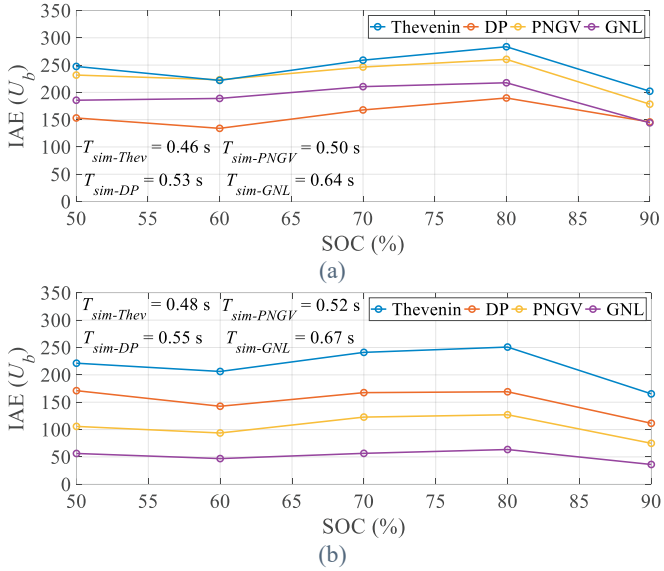

Figure 13. Integral absolute errors (IAE) of the battery ECMs with constant (a) and variable parameters (b)

As for the model complexity, the simulation execution time of the GNL model is about 40% longer compared to the Thevenin model and about 20%-30% longer compared to the PNGV and DP models. Interestingly, the PNGV model seems to be less computationally demanding than the DP model.

5. CONCLUSIONS

The analysis of four ECMs, carried in this study, has shown that the utilization of the Thevenin battery model can yield large errors in the open-circuit estimation of a lead-acid battery, both in steady state and during transients. If the ECM parameters are considered as constant, the DP model results in the smallest error, whereas the inclusion of the parameter variation has a significant favorable impact on the accuracy of the PNGV and GNL models. It was also shown that the addition of a series capacitance to the Thevenin model increases the ECM's accuracy to a greater extent than the inclusion of a second RC network. The GNL model with variable parameters, which is the most complex of the considered ECMs, has proven to be the most accurate, with about two times lower IAE value compared to the next most accurate, PNGV model. Of all the ECM variants considered, only the PNGV and GNL models with variable parameters have managed to provide a fairly accurate estimation of the open-circuit voltage, which is extremely important for applications where SOC or SOH estimation is considered.

REFERENCES

Castano, S., Gauchia, L., Voncila, E., and Sanz, J. (2015). Dynamical modeling procedure of a Li-ion battery pack suitable for real-time applications. *Energy Conversion and Management*, 92, pp. 396–405.

Chen, M. and Rincon-Mora, G.A. (2006). Accurate electrical battery model capable of predicting runtime and I–V performance. *IEEE Transactions on Energy Conversion*, 21 (2), pp. 504–511.

Chiu, H., Lo, Y., Lee, T., Chen, Q., Yu, W., Lee, J., Shih, F., and Mou, S. (2011). A battery charger with maximum power point tracking function for low-power photovoltaic system applications. *International Journal of Circuit Theory and Applications*, 39, pp. 241–256.

Doyle, M., Fuller, T.F., and Newman, J. (1993). Modeling of galvanostatic charge and discharge of the lithium/polymer/insertion cell. *Journal of The Electrochemical Society*, 140, 1526.

Du, J., Liu, Z., and Wang, Y. (2014). State of charge estimation for Li-ion battery based on model from extreme learning machine. *Control Engineering Practice*, 26, pp. 11–19.

Fang, H., Zhao, X., Wang, Y., Sahinoglu, Z., Wada, T., Hara, S., and De Callafon, R.A. (2014), State-of-charge estimation for batteries: a multi-model approach. *In Proceedings of the American Control Conference (ACC)*, Portland (OR), USA, pp. 2779–2785.

Haran, B.S., Popov, B.N., and White, R.E. (1998). Determination of the hydrogen diffusion coefficient in metal hydrides by impedance spectroscopy. *Journal of Power Sources*, 75 (1), pp. 56–63.

He, H., Xiong, R., and Fan, J. (2011). Evaluation of lithium-ion battery equivalent circuit models for state of charge estimation by an experimental approach. *Energies*, 4 (4), pp. 582–598.

Hu, X., Moura, S.J., Murgovski, N., Egardt, B., and Cao, D. (2016). Integrated optimization of battery sizing, charging, and power management in plugin hybrid electric vehicles. *IEEE Transactions on Control Systems Technology*, 24 (3), pp. 1036–1043.

Huang, T., Peng, R., Tsai, T., Chen, K., and Wey, C. (2014). Fast charging and high efficiency switching-based charger with continuous built-in resistance detection and automatic energy deliver control for portable electronics. *IEEE J. of Solid-State Circuits*, 49 (7), pp. 1580–1594.

Meng, J., Luo, G., Ricco, M., Swierczynski, M., Stroe, D.I., and Teodorescu, R. (2018). Overview of lithium-ion battery modeling methods for state-of-charge estimation in electrical vehicles. *Applied Sciences*, 8 (9), 659.

Moore, S. and Eshani, M. (1996). An empirically based electrosource horizon lead-acid battery model. *International Congress & Exposition*, Detroit (MI), USA, 960448.

Rahmoun, A. and Biechl, H. (2012). Modelling of Li-ion batteries using equivalent circuit diagrams. *Przegląd Elektrotechniczny*, 2 (7), pp. 152–156.

Unnewehr, L.E. and Nasar, S.A. (1982). *Electric Vehicle Technology*, Wiley: Hoboken (NJ), USA.

Zhou, W., Zheng, Y., Pan, Z., and Lu, Q. (2021). Review on the battery model and SOC estimation method. *Processes*, 9 (9), 1685.